GEOFIZIKA VOL. 42 2025

DOI: https://dx.doi.org/10.15233/gfz.2025.42.9
Original scientific paper

Geological structural mapping using aeromagnetic data to predict zones of rare earth minerals potential

Sunday Bayode [1], *Folahan Peter Ibitoye* [1,2] *and Ayokunle Adewale Akinlalu* [1,3]

[1] Department of Applied Geophysics, Federal University of Technology, Akure, Ondo State, Nigeria

[2] Prototype Engineering Development Institute, Ilesa, Osun State, Nigeria [National Agency for Science and Engineering Infrastructure (NASENI)]

[3] Department of Structural and Geotechnical Engineering, Polytechnic School, University of Sao Paulo, Brazil

Received 14 February 2025, in final form 18 July 2025

The application of aeromagnetic anomalies to rare earth mineral (lepidolite) exploration in Ijero-Aramoko pegmatite field Southwestern Nigeria, has been carried out with a view to determining the locations and depth to the lineaments hosting the pegmatite bodies. The methodology adopted involved Euler deconvolution technique applied to the 2-D profile and gridded potential field data to obtain estimates of locations and depths of causative bodies. In this study, upward continuation was applied to transform the aeromagnetic data, originally measured at a flight altitude of approximately 100 meters above ground level, to a height of 400 meters above sea level. This process allowed for the suppression of very shallow sources and background noise, thereby enhancing the imaging of relevant shallow magnetic sources (structures) and anomalies of interest in the residual aeromagnetic map. The 2-D geomagnetic sections developed along two section lines across the study area delineated suspected fault/fracture zones that are characterized by low magnetic susceptibility. Euler deconvolution method was applied to the data with SI values 0.5, 1 and 2. Euler solution for structural indices and the power spectral analysis gave depth values ranging from <10–50 m for shallow sources, 50–250 m for intermediate magnetic sources and 250–770 m for deeper sources. The Euler solution for structural indices of 0.5 and 1.0 gave the best solutions. The results of this study showed that pegmatite rich rare earth mineralisation occurs as a magnetic source which exhibited low magnetic intensity at relatively shallow depth. The existence of mining sites close to the lineaments further confirms the evidence of mineralisation of some the geologic structures delineated in the study area.

Keywords: lepidolite, Euler deconvolution, aeromagnetic, rare-earth minerals

1. Introduction

The growth of a nation's economy largely depends on a number of factors particularly the efficiency of the mining sector. In Nigeria, the position of the mining sector is in a bad shape. This can be attributed in large parts to government policies and the absence of reliable database of mineral resources in the country (Akande and Fakorede, 1988; Akinlalu et al., 2021; Akinlalu et al., 2024). This has resulted to the emergence of artisanal miners and the arbitrary exploitation of mineral deposits in areas suspected to be mineralized (KPMG, 2017). This in turn has a consequent effect on the environment as exploitation processes are often not conducted with world's best practices (Obaje, 2009; Gunn et al., 2018). Furthermore, targeted exploitation of the mineral deposits sought for is not achieved due to lack of information to guide exploitation. Consequent upon this, secondary deposits with lesser reserve than primary deposits are often tapped leaving largely the primary deposits with more potential less explored. This has grossly reduced the gross domestic product of the country as secondary deposits of less potential are often explored, contributing modestly to the economic growth of the nation (Obaje, 2009; Olade, 2019). However, to increase the mining potential of the country and its significant contribution to the economy of the nation, it is important to identify mineral deposits of primary origin (Allek and Hamoudi, 2008; Akinlalu et al., 2021; Akinlalu, 2023; Akinlalu et al., 2024; Olayanju et al., 2024; Sanusi et al., 2024; Akinlalu, 2025). Also, the rising demand for minerals, fueled by industrial growth and a rapidly increasing population, highlights the critical need to explore new potential mineral deposit zones to replenish exhaust reserves (Eldosouky et al., 2025).

This can be achieved by isolating localities of mineral occurrence and deposition by delineating geologic structures, lithologies and hydrothermal aureoles that permit the precipitation and eventual localization of mineral deposits (Andongma et al., 2021; Matende et al., 2023). These structures are products of tectonic events triggered by various chemical processes in the subsurface, hydrothermal alteration of the host rocks, and the development of diverse lineaments (Ekwok et al., 2022a; Liu et al., 2024a, b; Li et al., 2024a; Ordóñez et al., 2024). Identification of these structures and zones requires an extensive mineral exploration program (Yousefi and Carranza, 2016; Bai et al., 2021) involving geological, geophysical, geochemical and remote sensing methods of investigation (Behera et al., 2019; Riahi et al., 2022; Liu et al., 2022; Akinlalu et al., 2024). Systematic mapping of hydrothermal alteration haloes can help in indicating areas with potential for the discovery of mineral deposits (Eldosouky et al., 2024b).

Geophysics is generally recognized as a very vital method in the evaluation and exploration of economically viable mineral resources. The magnetic geophysical method is rated as a very sensitive and effective geophysical tool for prospecting mineralized zones especially when focused on areas of high struc-

tural complexity in magnetic data (Eldosouky et al., 2024a; Mahdi et al., 2025). Of these methods, geophysical and remote sensing methods offer a fast and precise way of targeted primary mineralization mapping. These methods are reliable in the delineation of structures controlling mineralization and in the mapping of lithologic units favoring mineralization. Recently, application of geospatial technologies has assisted significantly in increasing our knowledge of the earth and its hidden treasures (Alarifi et al., 2024; Eldosouky et al., 2024c). This is done by providing a way to gather data very quickly and convert it into important information. Furthermore, hydrothermally altered zones which contribute significantly to primary mineralization on a large scale can be delineated from these methods (Forson et al., 2020; Sanusi and Amigun, 2020; Zouaghi and Harbi, 2022; Akinlalu et al., 2024).

The use of geophysical methods ensures that subsurface structures genetically linked with primary mineralization are delineated with higher resolution. This is mostly accomplished using magnetic method.

Magnetic method of geophysical prospecting is a very important method in the search of base metals. It is also important in the mapping of basement geometry, depth to basement and structures guiding mineralization (Telford et al., 1990; Reeve, 2005). Filtering operations carried out on magnetic data like edge detection techniques involving analytic signal amplitude (*ASA*), total horizontal derivative (*THD*), tilt derivative, first vertical derivative (*FVD*), second vertical derivative (*SVD*), etc., in locating geological contacts and edges of structures controlling mineralization (Blakely, 1996; Nabighian, 1972). Also, depth estimation technique involving the 3-D Euler deconvolution ensures that geologic structures and their depth estimates are delineated using the appropriate structural index (*SI*) that gives the best-defined clustered solution (Matende et al., 2023; Afolabi et al., 2024; Akinlalu et al., 2024).

It is important to note that the study area is richly endowed with rare earth minerals such as lepidolite (lithium ore) (Okunlola et al., 2010; Akinola et al., 2014). Such minerals are found to be associated with deposits of pegmatite dykes, dyklets and quartz veins. According to Eberle et al. (2012) and Patra et al. (2013), these pegmatitic structures are characterized with linear structures/lineament features that can serve as a conduit that facilitates the accumulation of mineral resources in any area. The aforementioned structural linear features are either concealed at the near-surface or at deeper depth in the subsurface which makes the magnetic method of geophysical prospecting an ideal method to delineate those structures (Ajakaye, et al., 1986; Bayode and Akpoarebe, 2011; Uruc and Selim, 2011, Amigun et al., 2012; Eberle et al., 2012; Bayode, 2013; Patra et al., 2013; Olayanju et al., 2015; Wemegah et al., 2015; Oladunjoye et al., 2016; Bayode et al., 2023; Olomo, et al., 2024).

Based on the aforementioned, the applicability of the magnetic method of geophysical prospecting in the mapping of geological structural (lineament features) in a typical mineralized area is investigated. This is in a view to quanti-

tatively analyze and interpret aeromagnetic data towards deep seated linear structural features mapping and highlight their implications in mineral resources potential evaluation.

2. Description of the study area

The study area lies between longitudes 5°00' E and 5°06' E, and latitudes 7°46'9" N and 7°51'54" N (Fig. 1). The areal extent is about 137 km^2. Ground elevations in the study area vary from 400 to 610 meters (1300–2000 ft) above sea level, resulting in a nominal flight altitude of 400–710 meters above sea level (100 m above ground level).

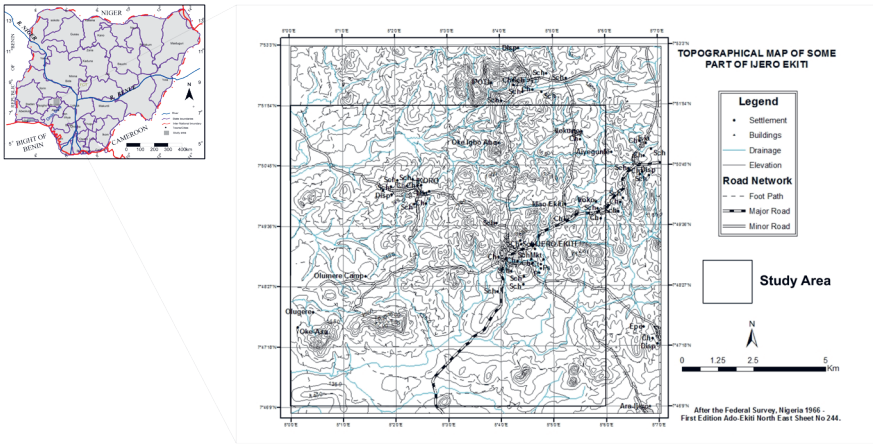

Figure 1. Location map of the study area (after Federal Survey, Nigeria, 1966).

2.1. Geology and mineralization

The Ijero-Ekiti area is underlain by the Basement Complex rocks of Southwestern, Nigeria. The local geology consists of migmatite gneiss, biotite gneiss, calc-gneiss, epidiorite, quartzite, biotite schist, amphibole schist, granite, basic dykes and pegmatite (Okunlola and Akinola, 2010) (Fig. 2). Migmatite-gneiss is the oldest rock underlying the study area. The migmatite gneiss occurs in the eastern part of the study area covering about one-third of the investigated area. The biotite gneiss predominantly covers the northwestern part. The biotite-gneisses are foliated with bands of black tints imposed by biotite impregnations alongside felsic minerals consisting of quartz and feldspar. The calc-gneiss is a typical gneissic metasediment rock with abundance of calcium. Epidiorite occurs as the major ultramafic rock in the investigated area. Quartzite occupies a narrow band in the NE–SW strip around Ijero-Ekiti town. Pegmatite dyke occur as

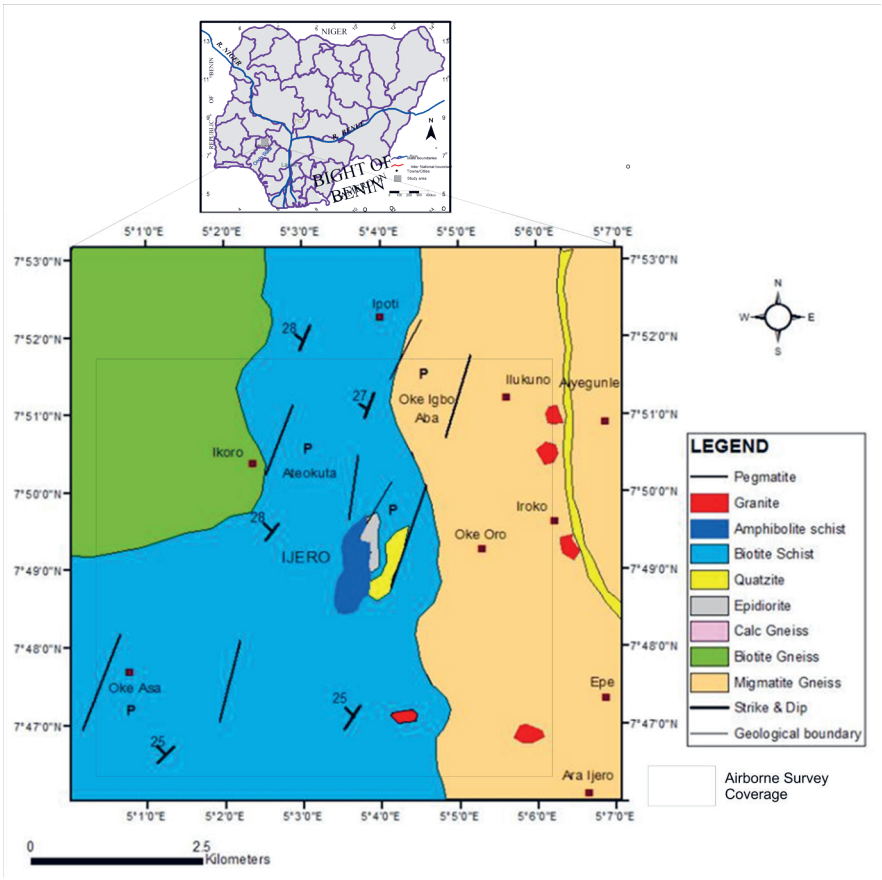

Figure 2. Geologic map of Ijero-Ekiti area showing the study area (after Okunlola and Akinola, 2010).

intrusions within the pre-existing rocks (migmatites, gneisses and biotite schist). Close to the centre of Ijero town, pegmatite occurs as very coarse grained dykes, veins, veinlets and sometimes with extensive dimension. The Ijero-Ekiti pegmatite is a rare earth metal type that is rich in lepidolite mineral as one of its constituent minerals (Okunlola and Akinola, 2010).

Pegmatites are intrusive rocks common to the entire Basement Complex rocks of the southwestern Nigeria, Ijero-Ekiti inclusive. The pegmatite intrusions have been found to be in close association with the pan-African granites that are associated with pronounced deformation and remobilization that occurred during the Pan-African orogeny about 650–450 million years ago (Odeyemi, 1976). The Ijero-Ekiti pegmatite field, which outcrops extensively as ridges within the pre--existing rocks has economic mineralization potential within the Basement Complex rocks of southwestern Nigeria. The pegmatites contain complex mineral assemblages which include; rare earth metals such as lithium (Okunlola and

Akinola, 2010); gemstones (blue and green tourmaline, aquamarine and topaz); raw materials for the glass and ceramic industry (quartz, feldspar, kaolin); and industrial minerals (mica). Field observations showed that there is an active mining activity going on within the study area and around Ijero at the time of this investigation for kaolin and green coloured tourmaline. Kaolin is mined for use in the ceramic industry while green tourmaline is mined for jewelry and ornamental purposes.

3. Method of study

3.1. Data acquisition and processing

In line with the recent need for improve revenue accruing from the mining industry into the Nigerian economy, efforts have been geared-up to improve mineral exploration and exploitation in the country. High resolution aeromagnetic data were acquired across the country between 2003 and 2009 by Fugro Airborne Survey Limited for the Nigerian Geological Survey Agency. The data analyzed in this paper were obtained in year 2006.

The airborne magnetic data covering North-West of Ado-Ekiti (sheet 244) constitute part of block B which was covered in the first phase of the project. The survey was carried out with a fixed wing (Cessna) aircraft. The Scintrex CS3 Cesium Vapour Magnetometer was used for the airborne magnetic survey. The sensitivity of the equipment is 0.0006 nT with noise envelope of typically 0.002 nT, 0.1 to 1 Hz bandwidth. The absolute accuracy is less than 2.5 nT throughout the range.

The survey has a tie-line spacing of 500 m, flight line spacing of about 100 m along a West-East direction and mean terrain clearance of 100 m. The survey line direction was approximately West-East and was made to be perpendicular to the main Nigerian Basement Complex rocks geological strike that is predominantly in the North-South direction. The aeromagnetic data were corrected for diurnal variation, heading error, system parallax, aircraft altitude and height variation effect.

The data-set was gridded with a minimum curvature gridding mesh size of 100 m and imported in to the Geosoft®, (2007) database. The projection method used in processing the data was the Universal Transverse Mercator (UTM) and the WGS 84, zone 31 of the North hemisphere as datum. The Spheroid model used was the Clarke, 1880 (modified), 33° E Central Meridian, a scaling factor of 0.9996, a 500,000 m *X* bias, a 0 m *Y* bias.

The aeromagnetic data-set was gridded to a 100 m interval so as to capture the anomalies properly using the minimum curvature technique described by (Briggs, 1974). The minimum curvature technique gridding was applied to the magnetic data. The minimum curvature technique takes the randomly distrib-

uted survey data and interpolates it to a regular grid as Total Magnetic Intensity (*TMI*) map. The images were produced in the Geosoft® (Oasis Montaj) software package. The filtering and data enhancement techniques were applied to improve the quality of the data for better understanding of the subsurface geology and its structural disposition. The MagMap extension in Geosoft®, which offers a number of utilities (filters) for processing of magnetic data, was used on the magnetic-anomaly grid for the processing and application of the filters. For this study, the advanced improved enhancement filters applied comprises the Fast Fourier transform filters which include Butterworth filter. The data enhancement technique applied are Reduction to Equator (*RTE*), Upward Continuation, First Vertical Derivative (*VDR*), Tilt Derivative (*TDR*) and Analytical Signal.

3.2. Reduction to magnetic equator (RTE)

Reduction to the equator is used in low magnetic latitudes to correct for latitude and to centre the peaks of magnetic anomalies over their sources. This can make the data easier to interpret while not losing any geophysical meaning. In this case, the magnetic field and magnetization will be horizontal as most of the magnetized sources. For the studied area, we prefer RTE to the popular Reduction to the Pole (*RTP*), which transforms the magnetic field and magnetization to a vertical orientation, effectively simulating a scenario where the geomagnetic field is purely vertical (as at the magnetic poles). Some RTP methods are numerically unstable at low magnetic latitudes due to the near-horizontal inclination of the Earth's field. Improved techniques, such as those proposed by (Keating and Zerbo, 1996), address these instabilities for low-latitude regions. In this study, RTE was applied to the TMI map with –10.0233° and –1.788° representing the inclination and declination respectively of the geomagnetic field parameters of the central location of the study area.

3.3. Upward continuation

The application of upward continuation in this work permitted the transformation of the aeromagnetic data measured from the flight altitude of 100 m to a height of 400 m above sea level to remove the effect of near surface noise. This produced a smoothing effect on the original data by attenuating short wavelength or high frequency anomalies relative to their long wavelength or low frequency counterparts (Langenhein and Jachens, 2014).

3.4. First vertical derivative (VDR)

The first vertical derivative is applied on magnetic data to enhance shallow wavelength features (shallow sources) that originate from near surface features while it suppresses the long wavelengths from deeper sources to yeild a better

and clearer picture of the subsurface geology. The first vertical derivative filter was applied to the reduced to equator *TMI* data to enhanced the local anomalies that may have been over-shadowed by the broader regional trend.

3.5. Tilt derivative (TDR)

The tilt derivative is highly suitable for mapping shallow basement structures and has distinct advantages over many conventional derivatives. The tilt derivative is defined by Miller and Singh (1994):

$$TDR = \tan^{-1}\left[\frac{VDR}{THDR}\right] \tag{1}$$

VDR and *THDR* represent the first vertical and total horizontal derivatives of the Total Magnetic Intensity (*TMI*).

$$VDR = \frac{dT}{dz}. \tag{2}$$

The *THDR* is defined by (Cooper and Cowan, 2008) as

$$THDR = \sqrt{\left(\frac{dT}{dx}\right)^2 + \left(\frac{dT}{dy}\right)^2}. \tag{3}$$

From Eq. (1), the amplitudes of the *TDR* are restricted to $-\pi/2$ and $\pi/2$.

3.6. Analytical signal

The amplitude of the Analytic Signal equals the square root of the squared sum of the two horizontal derivatives in the X and Y directions and the vertical derivative in the Z direction, as follows:

$$\left|A(x,y)\right| = \left[(\delta T/\delta x)^2 + (\delta T/\delta y)^2 + (\delta T/\delta z)^2\right]^{1/2}, \tag{4}$$

where:

A = analytical signal,

$\frac{\delta T}{\delta x}$ = horizontal derivative in X direction,

$\frac{\delta T}{\delta y}$ = horizontal derivative in Y direction and

$\frac{\delta T}{\delta z}$ = vertical derivative in the Z direction.

Analytic signal amplitude is widely used in magnetic interpretation for the determination of the location of the causative sources of the magnetic anomalies

(Roest et al., 1992; MacLeod et al., 1993a; Parlowski et al., 1995; Wijns et al., 2005; Cheyney et al., 2011).

3.7. Spectral depth-determination method

The Fourier transform of the potential field due to a prismatic body has a broad spectrum whose peak location is a function of the depth to the top and bottom surfaces and whose amplitude is determined by its density or magnetization. The relationship between the peak wavenumber (ω') and the body's geometry can be described as follows:

$$\omega' = \frac{\ln(h_b / h_t)}{h_b - h_t} \tag{5}$$

ω' is the peak wavenumber in radian/ground-unit, h_t is the depth to the top, and h_b is the depth to the bottom. For a bottomless prism, the spectrum peak at the zero wavenumber is according to the expression (Bhattacharya, 1966):

$$F(\mu,\nu) = e^{-hr}, \tag{6}$$

$$r = \sqrt{\mu^2 + \nu^2}, \tag{7}$$

where h is the depth to the top of the prism.

The spectrum for a prism with top and bottom surfaces is given as:

$$F(\mu,\nu) = e^{-h_t r} - e^{-h_b r}, \tag{8}$$

where ? and ? are the angular wavenumbers in radians/ground-unit, h_t and h_b are the depths to the top and bottom of the prism respectively.

When considering a line that is long enough to include many sources, log spectrum of these data can be used to determine the depth to the top of a statisticalensemble (assemblage) of sources using the relationship (Spector and Grant, 1970) as shown in Eqs. (9) and (10):

$$\log E(k) = 4\pi hk, \tag{9}$$

where, h is the depth in ground-units and k is the wave number in cycles/ground-unit.

The depth of an "ensemble" of source can be determined by measuring the slope of the energy (power) spectrum and dividing by 4π, as expressed below:

$$h = -\frac{s}{4\pi}(-), \tag{10}$$

where h is depth and s is the slope of the log (energy) spectrum.

The above estimates can be used as a rough guide to the depth of magnetic source populations.

A typical energy spectrum for magnetic data may exhibit three parts: the deeper sources component with longe wavelength and decay away slowly, the shallow sources component with shortwavelength, which dominate the short wavelength end of the spectrum, and a noise component.

3.8. Euler deconvolution

The aeromagnetic data were interpreted using the 3-D Euler Deconvolution algorithm in Geosoft® (Oasis montaj) software for location and depth determination of causative anomalous bodies from gridded potential field data. In Standard Euler Deconvolution method, the solutions were calculated within a fixed window size. The square window moves over every data point in a uniform grid and produces a large number of solutions all over the grid. The Euler deconvolution as applied at each solution involves setting an appropriate Structural Index (SI) value and using least-squares inversion to solve the equation for an optimum x_0, y_0, z_0, and total magnetic field intensity (B). The Euler deconvolution method relates the vertical and horizontal gradient of the residual magnetic intensity values with help of geometry of the magnetic bodies given by the SI (Thompson, 1982 and Barbosa et al., 1999).

The window size and the respective number of the observation points, for which the system of linear equations is formed are also parameters in solving the inverse magnetic problem. Window size of 10 m prove to be most suitable in this study and was used.

Solutions with depths to source below the error tolerance levels were rejected. A real data set is likely to contain anomalies from sources with various structural indices. It is, therefore, necessary to solve for a range of indices values

Table 1. Summary of structural indices for simple model in a magnetic field (Reid et al., 1990).

Magnetic model	Characteristics	Number of infinite dimensions	Magnetic SI (Structural Index)
Sphere	Occurs as sphere bodies of circles with a common axis connecting them	0	3
Pipe (vertical cylinder)	Occurs like a vertical pipe and circles intertwined neatly with regular circumference	1 (z)	2
Horizontal cylinder			2
Dyke (thin prism with large circles)	Circles are intertwined in a straight line	1 (x–y)	1
Sill			1
Contact with small extent	Circles are intertwined in a pattern that is linear and in rows	0	0.5
Contact with large extent	Circles are intertwined with no particular pattern	0	0

of 0.5, 1.0 and 2.0 and to plot the results for each index. The maps are then examined feature by feature and the index which gives the best solution clustering is chosen for each feature. The relationship between the *SI* values and the geologic model (geometry) is presented in Tab. 1. This procedure also gives some clue to the nature of the source geometry, geologic features and boundaries.

4. Results and discussions

4.1. Total magnetic intensity (TMI) map

The Total Magnetic Intensity (TMI) values obtained for Ijero-Ekiti area corrected for the core field generally show amplitude values which range from –3.87 to 98.67 nT (Fig. 3). The variation in the amplitude of signal reflects the aniso-

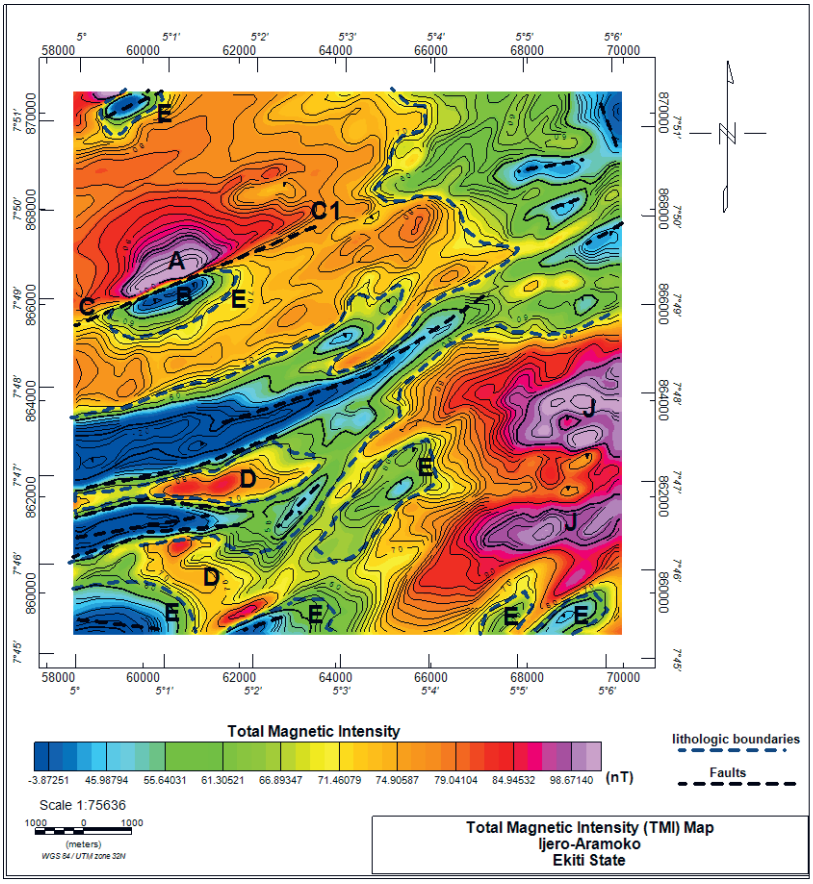

Figure 3. Anomalous Total Magnetic Intensity (*TMI*) of the study area showing the faults and lithologies.

tropic nature of the basement rocks. Careful examination of the TMI map with the geological map of the study area (Fig. 2) suggests that the observed lithologic units include migmatite gneiss, biotite gneiss, amphibolites schist, biotite schist, epidiorite and granite. The north-western part of the TMI map (Fig. 3) is characterised by relatively high magnetic intensity values which range in values from 71.46 to 98.67 nT and appear to coincide with the biotite gneiss rock unit (Fig. 2). Similar anomaly is observed at the southeastern part of the map. This reflects the migmatite gneiss rock unit which displayed low amplitude and long wave length anomaly pattern in the northwest and southeastern part of the TMI map. This is an indication of deep nature of the basement in the study area. The relatively low magnetic intensity values in the range of –3.87 to 66.84 nT coincides with the areas where biotite schist is located on the geological map (Fig. 2). Although, few of these relatively low magnetic intensity values still fall within the migmatite gneiss, this may be attributed to a gradation between the migmatite gneiss and the schist. In low magnetic latitude region, specifically around the equator within southwest area low/negative magnetic peak values represents typical anomalous signatures.

The map revealed prominent low/negative amplitude (dark blue colour bands) features in circular and elongated shapes found in the southwestern, central and northeastern parts of the study area. Presence of NE–SW trending lineaments in the study area was reported by (Okunlola and Akinola, 2010). Basement lineaments (faults/pegmatite dykes) include C–C_1, trending approximately NE–SW which are also observed on the TMI map.

This fault C-C_1 cut across the biotite gneiss rock unit in the north-western part of the study area as shown in the geological map (Fig. 2). However, the anomaly J in the southeastern part of the map is suspected to be indicative of the presence of low magnetic bodies (such as granitic rocks) which intruded into the pre-existing migmatite gneiss rock unit found in the eastern part of the study area (Fig. 2).

4.2. The residual map

Figure 4 shows the residual magnetic map which display the intensity and the wavelength of local anomalies. The magnetic anomalies correlate with the expected magnetic signatures of the migmatite gneiss, biotite gneiss, amphibolite schist, biotite schist, epidiorite and granite where mafic and felsic rocks are represented by high and low amplitude magnetic anomalies rocks are represented by high and low amplitude magnetic anomalies biotite gneiss and epidiorite (areas with high magnetite mineral content) while the low magnetic regions characterized by (green – deep blue colour bands) in the SW which extended to the NE part are located around the amphibolite schist, biotite schist, and granitic bodies (areas characterized with low magnetite mineral content due

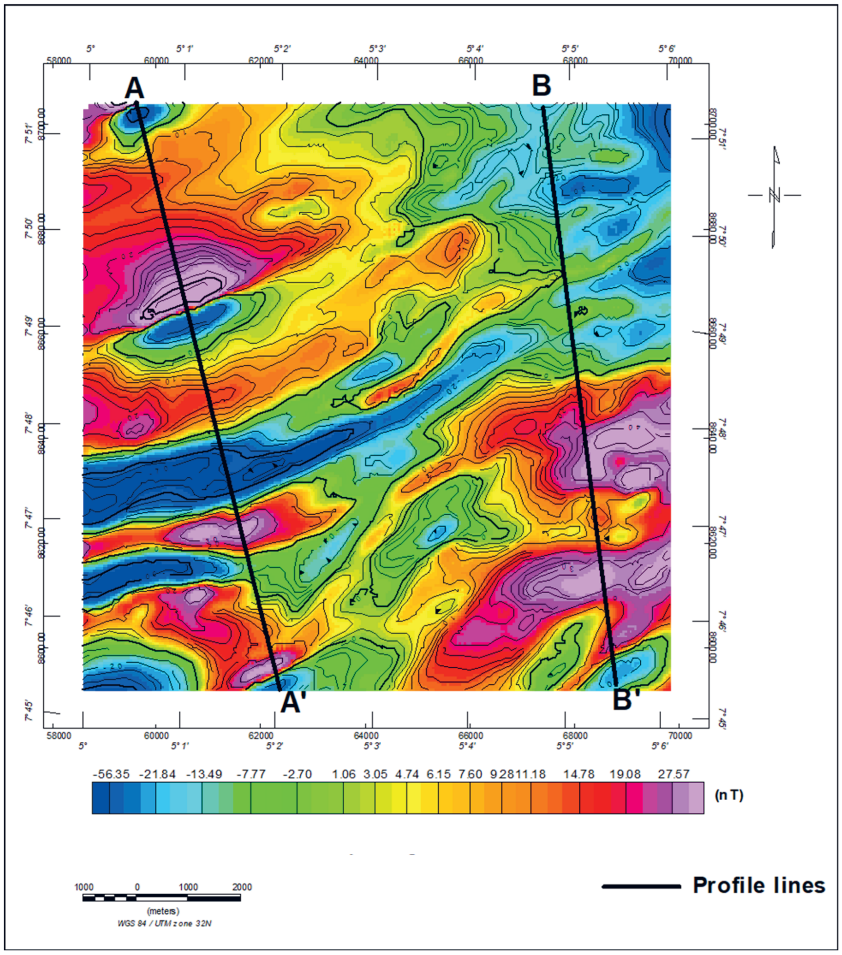

Figure 4. Residual aeromagnetic map of the study area.

to low iron forming minerals). The observed anomaly patterns are similar to that of the TMI and RTE maps.

The *TMI* data was further upward continued to a height of 12 km in order to remove response from deep seated structures (Fig. 4). Two profiles A–A´ and B–B´were drawn to be approximately perpendicular to the strike direction of the contours of the residual map of the study area (Fig. 4). Figures 5 and 6 show the two profiles and the corresponding geomagnetic sections A–A´ and B–B´ generated across the residual map. The profile anomalies reflect the structural features (fracture, faults and geologic boundaries/contacts) along the profiles. The geomagnetic sections developed for the study area revealed that depth to magnetic basement in the investigated area range from about < 2.5–50 m and may

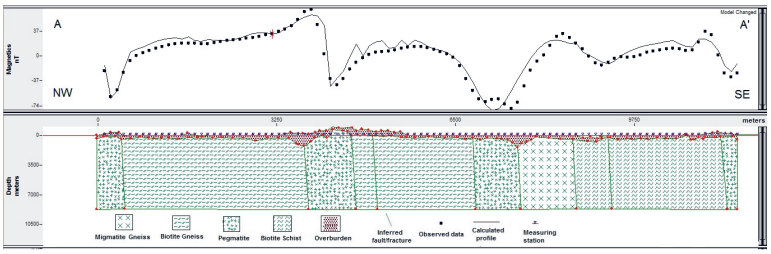

Figure 5. Magnetic profile and corresponding geomagnetic section along profile A–A´ and within the study area.

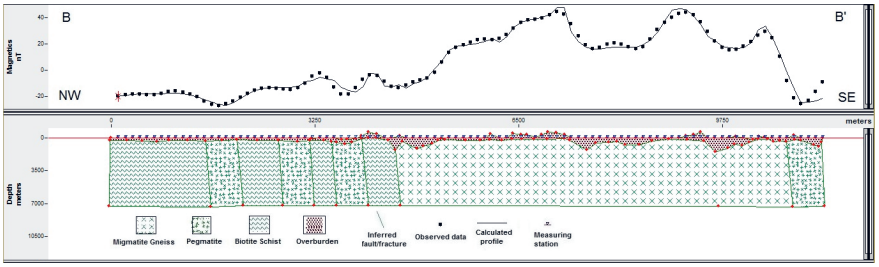

Figure 6. Magnetic profile and corresponding geomagnetic section along profile B–B´ within the study area.

be up to 100 m in places within the study area. The geomagnetic sections were able to delineate some identified geologic structures (fault/fracture) zones suspected to be hosting pegmatite dykes along the profiles (Figs. 5 and 6).

4.3. Derivative map

4.3.1. The reduction to equator (RTE) map

The Reduction to Equator (*RTE*) map (Fig. 7) shows similar trends and patterns as shown in the Total Magnetic Intensity (*TMI*) map (Fig. 3). This includes anomalies marked A, B, D and J which were both observed in the RTE and the Total Magnetic Intensity (TMI) maps (Figs. 3 and 7). The identified anomaly labelled E in the Total Magnetic Intensity (TMI) map is also observed in the Reduction to Equator (RTE) map, but it is more clearly defined in the Reduction to Equator (RTE) map (Fig. 7). The instantaneous stress drop is the change in the stress on the fault plane at the moment at which an event occurs and is theoretically defined as the difference between the initial stress (before the event) and the termination stress (after the event). Among events with similar magnitudes, the larger the stress drop is, the higher the source stress of the event. Therefore, the local environmental stress of the source area can be roughly determined based on the magnitude of the stress drop of the event (Pulido et al.,

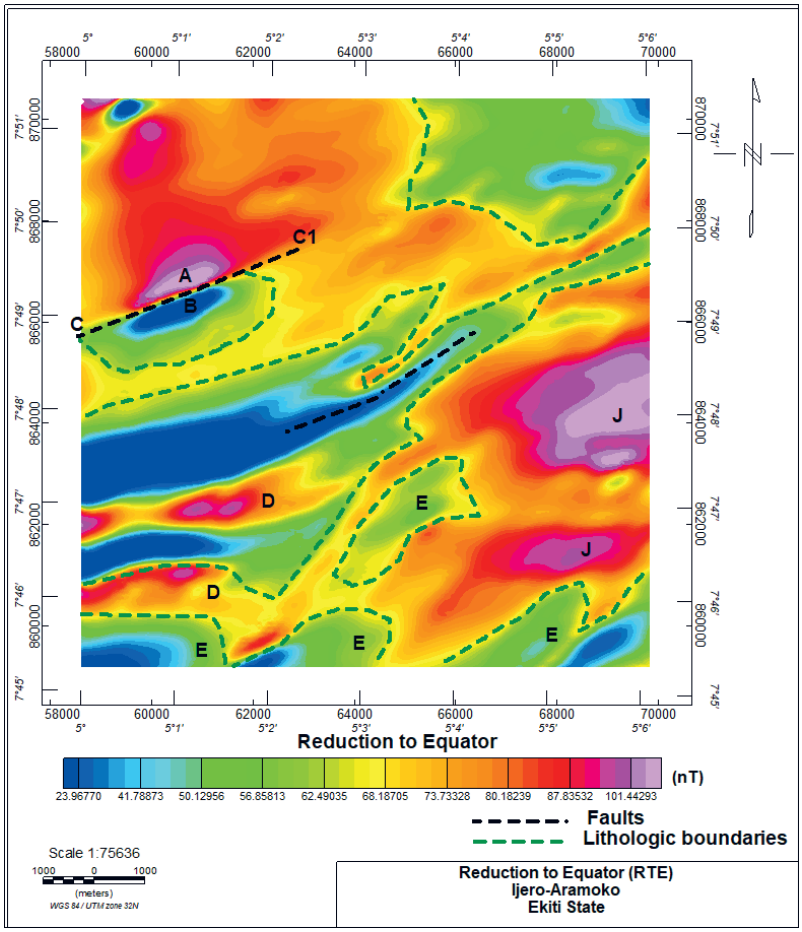

Figure 7. Reduction to equator (RTE) map of the study area.

2000; Jiang, 2015). The stress drops of the mining tremors in this study were relatively low, ranging from 0.02 to 0.18 MPa (Tab. 1), indicating that these strong mining tremors essentially occurred under relatively low environmental stress conditions.

4.3.2. Upward continuation map

Figure 8 is the upward continuation map of Ijero-Ekiti area. A fault C–C_1 trending NE-SW direction occurs along the narrow boundary that exists between the high amplitude anomaly marked A and the low amplitude anomaly marked B (Fig. 8). The observed anomalies A and B are suspected to fault C–C_1 that was earlier delineated on the Total Magnetic Intensity (TMI) map in terms of location and orientation.

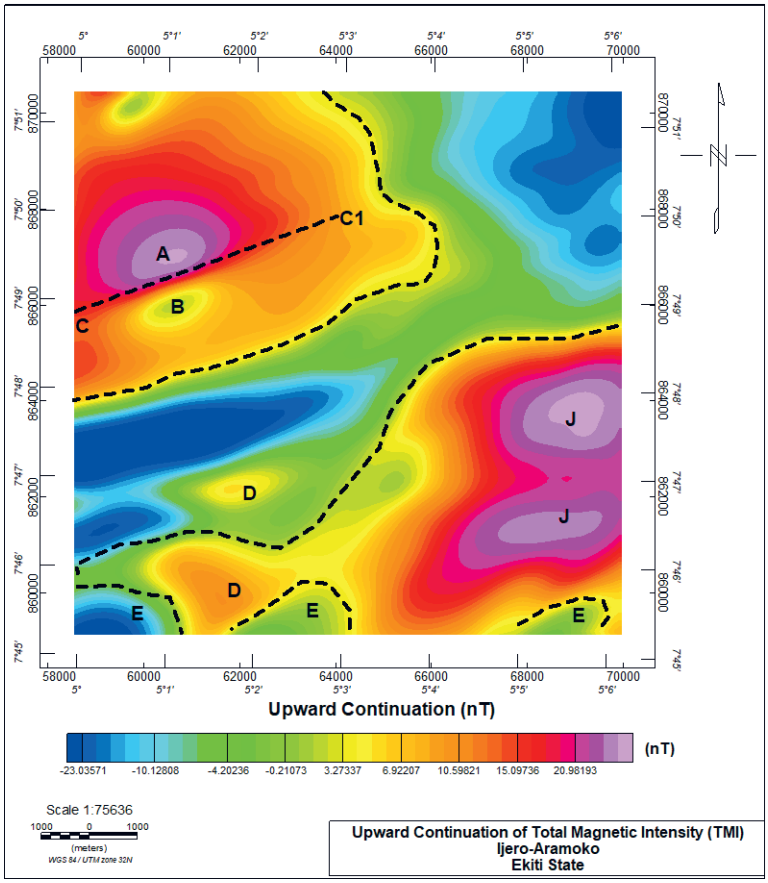

Figure 8. Upward continuation map at a depth of 400 m in the study area.

This implies that the identified fault C–C_1 is probably a deep seated large scale fault. This fault may define the principal orientation of the tectonic setting of the study area. The low/negative anomalies comparison of the upward continuation map (Fig. 8) with the Total Magnetic Intensity (TMI) map (Fig. 3) of the study area show prominent anomalies marked A, B, and J which are suspected to be due to deeper magnetic sources within the study area. The high magnetic intensities observed at A and B are suspected to be due to the effect of a dissected composite (single) prismatic body (dyke) while anomalies J (Fig. 8) is the same as observed in (Fig. 3) with similar interpretation as earlier observed above in the TMI and RTE maps.

4.3.3. The first vertical derivative map

The first vertical derivative (FVD) map helps to enhance local and short wavelength anomalies. It was applied to the Reduction to Equator (RTE) map

(Fig. 9). The figure shows that the short wavelength anomalies marked D that are not seen clearly in the Reduction to Equator (RTE) map, are more visible on the first vertical derivative of the RTE map. The major fault C–C_1 in (Fig. 9) coincides with the identified fault C–C_1 in the Total Magnetic Intensity (TMI) map (Fig. 3).

This fault as earlier observed is responsible for the disection of a suspected prismatic dyke body into two as displayed in the TMI map of the study area (Fig. 3). An anomaly labeled E located between anomaly J in the southeastern part,which appear to be an extension of anomalies E located westward in the south--central part (Fig. 9) is noticed to be absent in the Reduction to Equator (RTE) map. The anomalies labelled E in the first vertical derivative of the Reduction to Equator (RTE) map (Fig. 9) can be inferred to be short length geological features.

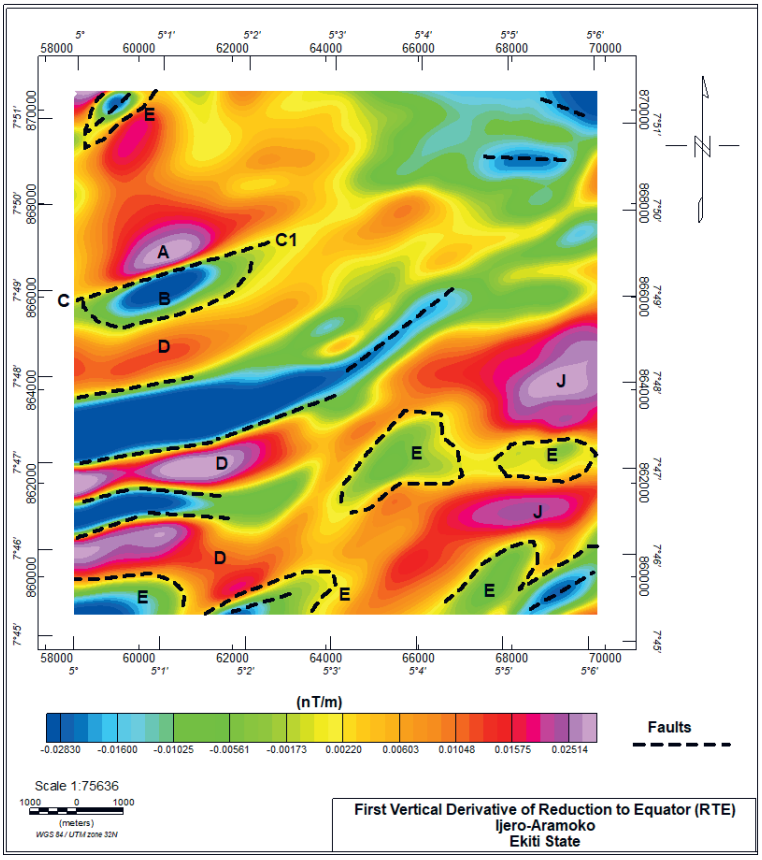

Figure 9. First vertical derivative of reduction to equator (RTE) map of the study area.

4.4. 3-D Euler deconvolution of aeromagnetic data

The results of the 3-D Euler deconvolution are presented as maps (Figs. 10, 11 and 12). These maps show the solutions that passed the specified acceptable tolerance. The structural indices of 0.5 and 1.0 are quite similar for the study area (Figs. 10 and 11). Figures 10, 11 and 12 show the estimated source positions and depth values for structural indices of 0.5, 1.0 and 2.0 respectively in the study area. The centre of the plotted circles represents the plan location (x_0, y_0) of the interpreted source and diameters of the plotted circles are proportional to the depth values. The depth estimates are displayed using colour variations to represent different range of values. The 3-D Euler solutions were superimposed on the Total Magnetic Intensity (TMI) map in order to correlate the geologic structures delineated on the TMI map and the 3-D Euler solutions at different structural indices.

The Euler solutions of SI values of 0.5 related to (contact) and 1.0 typical of (dyke and sills) as shown in Table 1 appear to have a satisfactotry match with noticable clusters around some anomalies and hence were accepted as solutions (Figs. 10 and 11). The intertwined/non linear clusters located in the central part

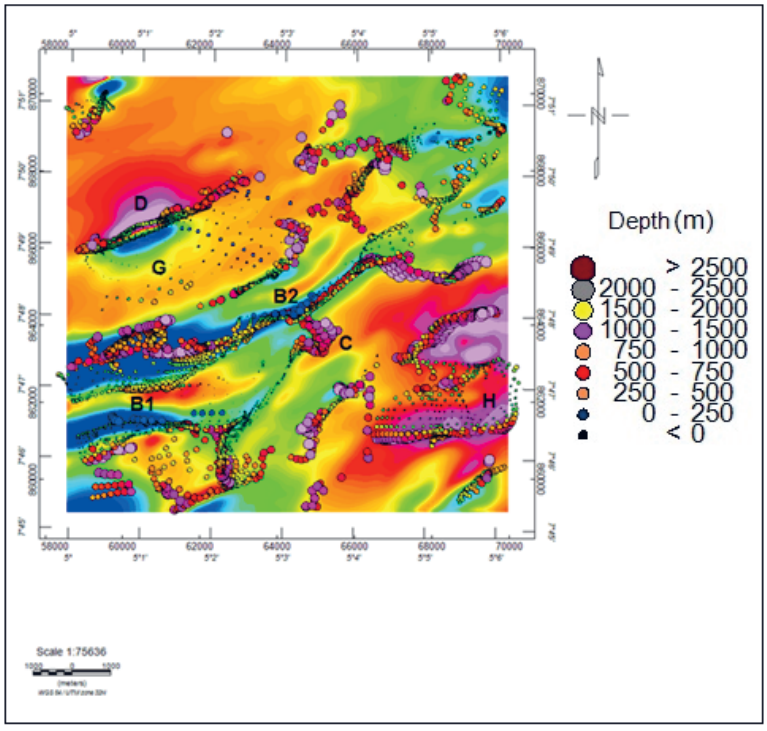

Figure 10. 3-D euler deconvolution results of map of the study area for structural index of $N = 0.5$.

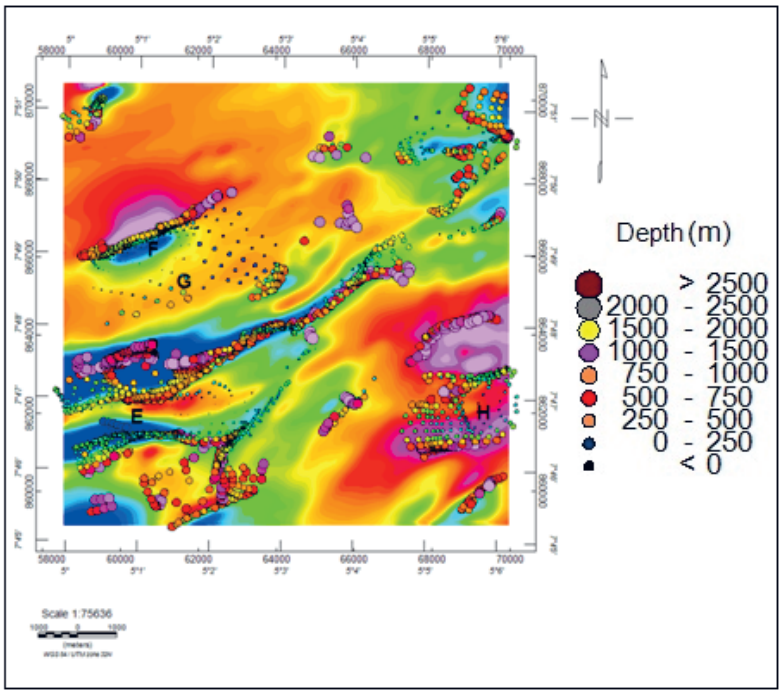

Figure 11. 3-D Euler deconvolution results of structural index ($N = 1.0$) map of the study.

which extends to the west and the southern part of the map suggest geological contacts while the linear clusters observed in the southwest, central, southeast, northeastern and northwestern part of the maps (Figs. 10 and 11) can be inferred to depict the presence of geologic structures/lineaments in the study area. The Euler solutions for shallow depth sources for structural index (SI = 0.5 and 1.0) of the magnetic anomalies (geologic features) over the study area (Figs. 10 and 11) have depth values which ranges from 0 to 250 m.

The solutions for intermediate depth sources range from orange to red colour bands (250–500 m) while the relatively deep depth sources ranging from red to magenta colour bands (500– > 1000 m) are located mainly at the northwestern, northeastern, central, southwestern and southeastern part of the map (Fig. 10), where high magnetic intensities were observed. These Euler solutions coincide with biotite schist, migmatite gneiss and biotite gneiss rock units within the study area. The distributions and clustering of some solutions fall along the edges of the lithologic unit. The solutions for relatively shallow depths sources shown in light blue colour to dark blue colour bands marked B1 and B2 (0–250 m) are located in various part of the investigated area (Fig. 10). The anomaly mark B1 located at the southwestern part of the map (Fig. 10); coincides with a fault around which mining activity is centered at Oke- Asa in the neighbourhood (see

Fig. 2). A cluster of linear solutions in form of a straight line in the northwestern part marked D is approximately parallel to the one located in the southwestern and central part of the map marked B1 and B2. This can be inferred to be a twin replica of the body observed northward, and are probably a product of the same dislocation boundary or fault which may be associated with the same tectonic event.

The observed Euler solutions is suspected to be characteristic of low magnetic intensity zones (blue colour band) in the map (Fig. 10), which coincides with the location of suspected pegmatite bodies in the map, as shown in the geological map of the study area (Fig. 2). A circular cluster of solutions at a depth range of 500 to 1000 m marked C in red to magenta colour bands located at the central part of the map (Fig. 10), is observed to coincide with the assemblage of amphibolite schist, epidiorite and quartzite rock units (Fig. 2). A cluster of linearized solutions in the north-western part of the map (Fig. 10) marked D is observed to be suggestive of a lithologic boundary/fault which are found to correlate very well with the anomaly patterns that are oriented in the (NE-SW) directions, typical of the Nigerian Basement Complex structural disposition that can be interpreted as lineaments hosting pegmatites that are suspected to be impregnated with rare earth minerals (lepidolite). This is also observed to coincide with the cluster

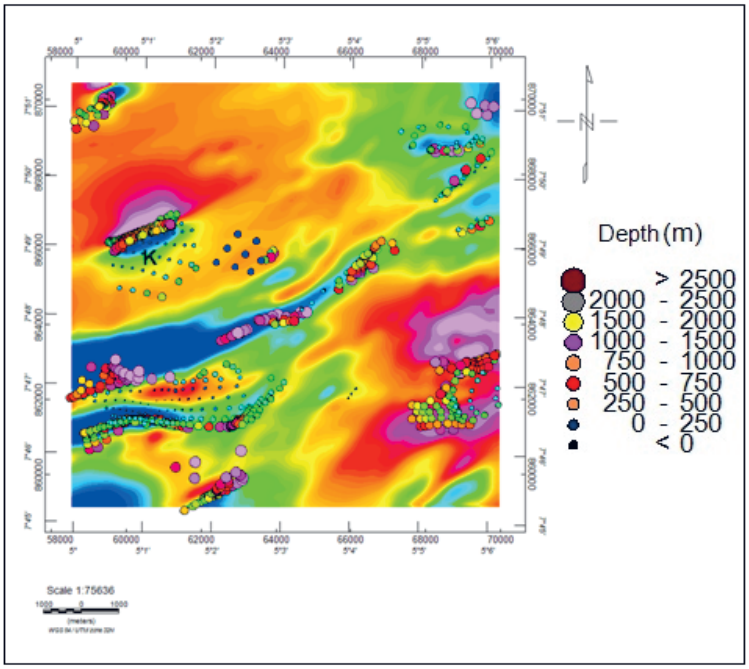

Figure 12. 3-D Euler deconvolution results of map of the study area for structural index of $N = 2.0$.

of solutions delineated on the Euler solutions for Structural Indices (SI = 1.0 and 2.0) (Figs. 11 and 12). Also, the observed scattered clusters of solutions (circles) marked 'H' (Fig. 10) was also noticed at the southeastern part of the map, and it coincides with the intruded granite body exposure (suspected to have a wider spread at depth than the surface expression) shown at a similar location in the geological map of the study area (Fig. 2).

4.5. Estimate of depth to basement

Figure 13 (a and b) shows a plot of the calculated spectral analysis and the radially average power spectrum plot for the study area. The power spectral analysis of the aeromagnetic data revealed three depth source models. Three gradients are shown in (Fig. 13) which corresponds to linear segments of the power spectrum. The high gradients are related to the deeper sources, the medium gradient is indicative of the intermediate depth sources while the low gradients are related to the shallow sources. The first magnetic layer (shallow sources) (Fig. 13a) which dominates the high wavenumbers (Fig. 13b) could be attributed to the effect of near-subsurface mineralized bodies (pegmatite dykes and veins), supergene ore enrichment blankets, gossans and other magnetic minerals that may have been released into decomposed rocks (reddish clay-rich

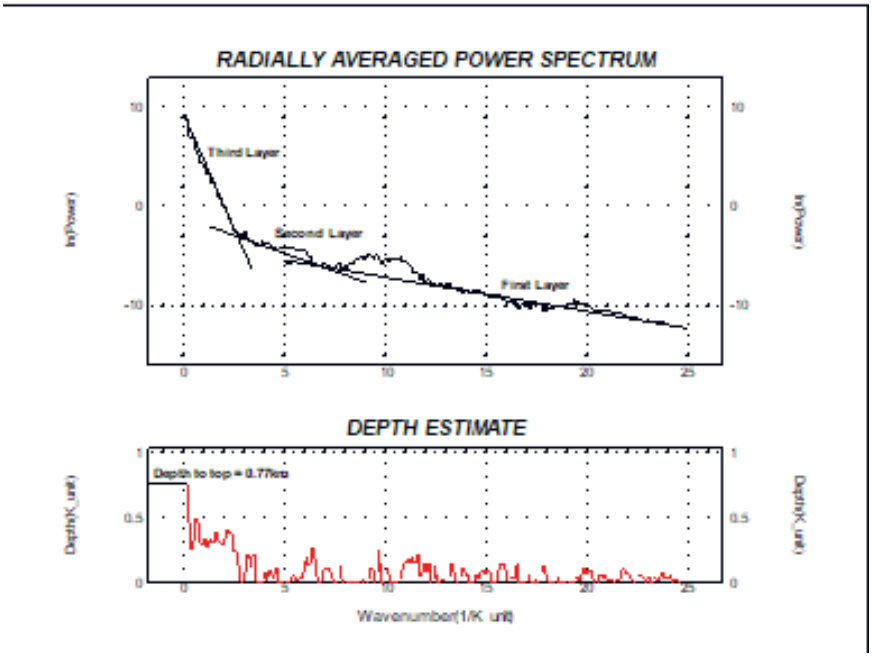

Figure 13. (*a*) Radial spectrum, (*b*) Depth estimate plot.

zone in muscovite, kaolinized feldspar, quartz, lepidolite, and tourmaline) which are present in the near-subsurface layer. The shallow magnetic sources range in depth from about < 10–50 m. The second magnetic layer (intermediate deeper sources) (Fig. 13a) which dominates the intermediate wavenumbers (Fig. 13 b) is suspected to be intrusive rocks that are rich in magnetic minerals (pegmatite and granitic vein bodies) into the parent rock (migmatite gneiss and schists) that are characterized with lateral discontinuities in the basement magnetic susceptibilities and basement geologic features such as faults, dykes and lithological contacts. The depth to the intermediate magnetic sources ranges from about 50–250 m (Figs. 13a,b). The depth to the top of deepest magnetic sources ranges from about 250–770 m as shown in Figs. 13a,b. The depths to magnetic sources at Ijero-Ekiti area range from < 10–770 m. The depth values of < 10–770 m obtained from the radially average power spectrum plot for the study area correlate well with the estimated depth values obtained from the Euler deconvolution for SI of 0.5 and SI of 1.0. Therefore, the structural index of 0.5 (contacts) and 1.0 (dykes and sills) is considered to be more acceptable magnetic model for the study area.

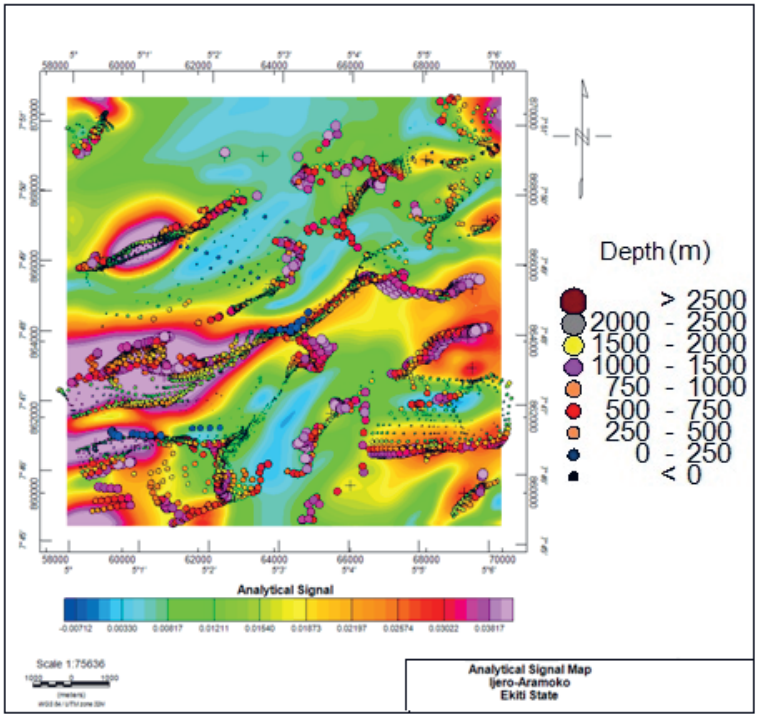

Figure 14. Analytical signal map of the study area.

4.6. Analytical signal map

The analytical signal map (Fig. 14) shows the maxima amplitude (magenta colour band) indicated by a cross located at the edges of the geological boundaries and some intrusive bodies (granites and pegmatite dykes). The tightest clustering of solutions obtained from the Euler deconvolution for structural index (SI) of 0.5 and 1.0 generally coincides with the maximum amplitudes of the analytical signal (Fig. 14). This validated the Euler solutions and implies that some of the intertwined circles in a pattern that is linear and in rows found in the northeast, southwest, southeast and northeastern part of the study area delineated by the Euler solutions (Figs. 10 and 11) are actually geologic structures contacts/lineaments. Figure 14 shows the Euler solutions for structural index (SI) of 0.5 superimposed on the analytical signal. This includes a major long stretched high amplitude anomaly (magenta colour band (Fig. 14)) located between latitudes 7° 47^{l} N – 7° 47.6^{l} N (southwestern part), which coincides with the previously delineated light blue to deep blue colour band low/negative amplitude anomaly in the Total Magnetic Intensity (TMI) map (Fig. 3) that majorly aligned Northeast–Southwest directions in the study area were delineated. Tight clustering of solutions was observed at the edges of irregular anomalies, this could be inferred to be the edges of geologic boundaries/contacts between the biotite gneiss and biotite schist in the southwest, and the biotite schist and migmatite gneiss rock units observed at the north-central part which extends to the eastern part of the study area.

4.7. Structural interpretation of Euler solutions

The Euler solutions for structural indices of 0.5 and 1.0 are similar and gave the best solutions since they have the circles that are intertwined in a straight-line pattern and same orientations in the study area. The structural index of 0.5 and 1.0 give the tightest cluster of solutions (circles) as observed in Fig. 15. Figure 15 shows that the central, extending to the northeast and southwestern parts of the study area are more densely fractured than the northwest and southeastern part of the study area. The observed structural trend is mainly oriented in the NE–SW directions while a few ones in the southeastern part are aligned in an approximately E–W directions. The structures that are oriented in the NE–SW directions were observed to mimic the existing geological trends within the Nigerian Basement Complex. The 3-D Euler Deconvolution results of the study area for structural indices of 0.5 and 1.0 gives depth to the structural bodies at relatively shallow depth value of < 10–50 m. The intermediate depth is 50–250 m while the deep depth is observed to be about 250–700 m. The observed lineaments in (Fig. 15) can be interpreted to be geological structures (fault/fractures/geological contacts) that are suspected to be host for rare earth metal mineralization in the investigated area.

The geologic structures (faults, fractures, sheared zones and lithological contacts) were delineated along the best clusters of solutions (circles) (Fig. 15). Clusters of solutions (bluish colour band) at relatively shallow depth range with values which vary from 0–250 m are located at the northeastern, western, central, eastern and southwestern part of the study area (Fig. 15). These locations coincide with Oke-Asa and Ijero pegmatite bodies as shown in the geological map (Fig. 2). Akinola et al. (2014) observed that the Ijero-Ekiti pegmatite deposit features two levels of lepidolite mineralisation; an upper layer 1.2 m thick and a lower layer 2.4 m thick are separated by a layer of gritty kaolin deposit resulting in their occurrences at depths of 8 m and 11 m respectively in the investigated area. The Ateokuta pegmatite is located at about 500 m northwest of Ijero town (Fig. 2). It features a single layer of lepidolite mineralization; the thickness is 5.1 m, and it occurs at a depth of 10 m. The depth to lepidolite mineralization at Oke-Asa pegmatite deposit was not specified as earlier observed by (Akinola

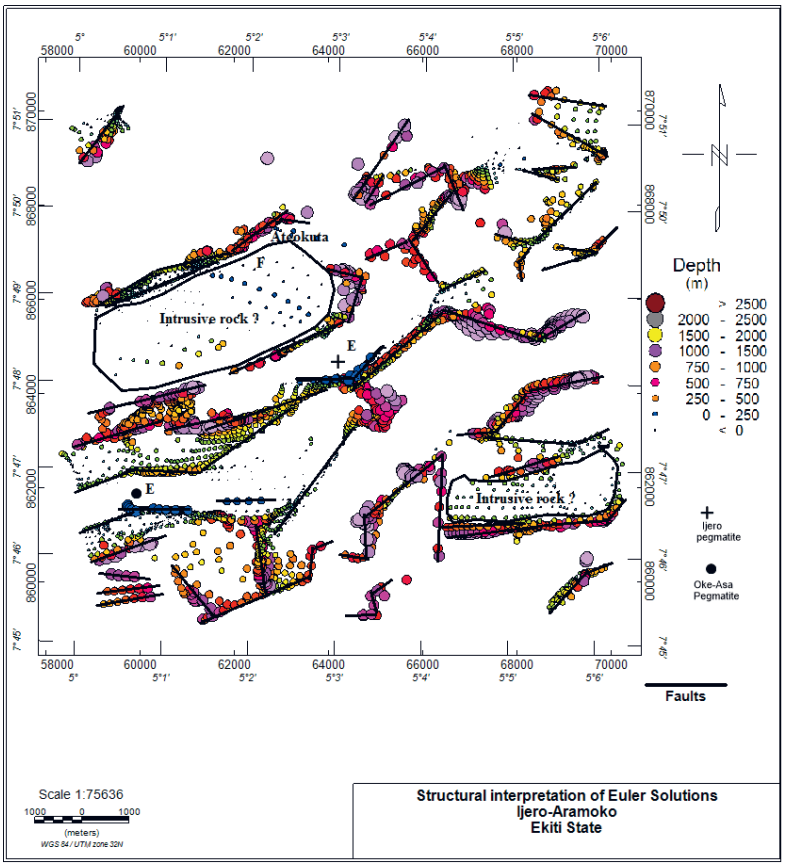

Figure 15. Structural map interpretation of the euler solutions of the study area.

et al., 2014). From the above deductions, the depths to lepidolite mineralisation of 8, 10 and 11 m given by Akinola et al. (2014) for Ijero-Ekiti and Ateokuta pegmatite bodies fall within the shallow depth range of 0–250 m that was obtained from the Structural Interpretation of the Euler Solutions for the investigated area, this implies that lineaments bearing rare earth minerals (such as lepidolite) occurs as a magnetic source at a shallow depth range of values 0–250 m in the study area, and also, exhibited as low magnetic intensity at the locations. The Ateokuta pegmatite body could not be delineated in this study due to the scattering of solutions around the location marked 'F' (Fig. 15), it is suspected to be an intrusion of pegmatite bodies into the parent rock (schist). According to Akinola et al. (2014), amphibole schist and biotite schist occupy the central low-lying areas of the investigated area with occurrence of intrusive granites and pegmatite bodies, now exposed or outcropping due to prolonged weathering and erosion activities within the study area.

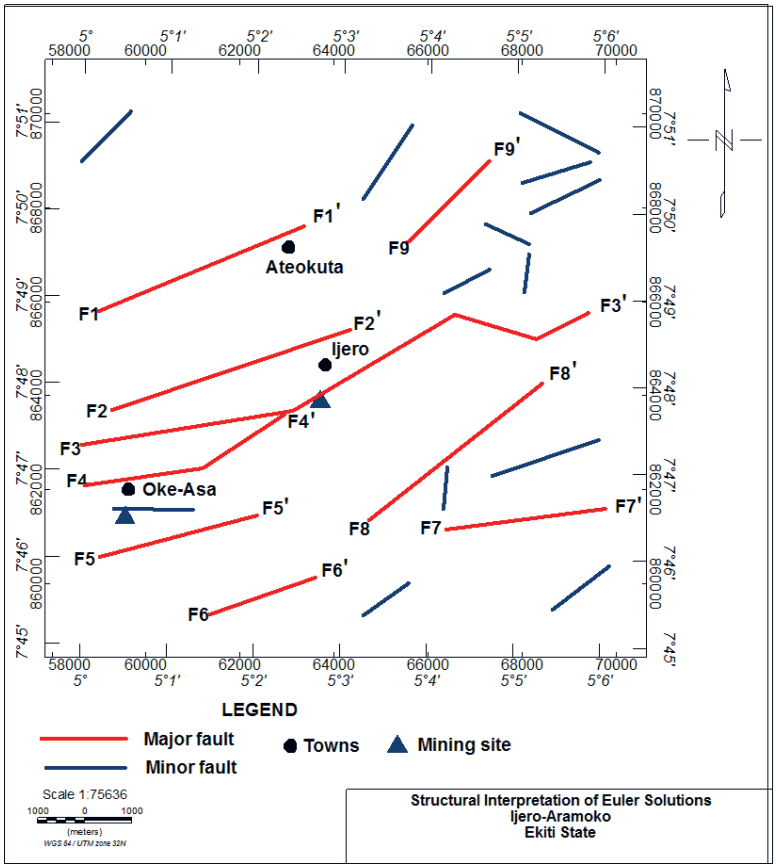

Figure 16. Developed structural map of the study area.

Figure 16 show the developed structural map of the study area. The major lineaments were observed to generally trend in the NE–SW directions similar to the occurrence of pegmatite dykes in the study area. This suggests that both the observed geologic structures and the pegmatite bodies are probably affected by the same tectonic event during their emplacement in the investigated area. Minor lineaments are observed to trend east – west and northwest – southeast directions (Figs. 15 and 16). The location of the existing mining sites (Fig. 16) close to/along the lineaments is indicative of mineralisation of some geologic structures in the study area.

5. Conclusions

The Anomalous Total Magnetic Intensity (TMI) values obtained for the Ijero-Ekiti area, following correction for the core field, exhibit amplitude values ranging from –3.87 to 98.67 nT. These variations in amplitude reflect the anisotropic character of the basement rocks within the study area. Careful examination of the TMI map with the geological map of the study area suggests that the observed lithologic units include migmatite gneiss, biotite gneiss, amphibolite schist, biotite schist, epidiorite and granite. The north-western part of the TMI map is characterised by relatively high magnetic intensity values which range in values from 71.46 to 98.67 nT. This appears to coincide with the biotite gneiss and migmatite gneiss rock units. The relatively low magnetic intensity values in the range of –3.87 to 66.84 nT coincides with the areas where biotite schist is located in the study area. The map also revealed prominent low/negative amplitude (dark blue colour bands) NE–SW trending lineaments features located in the southwestern, central and northeastern parts of the study area.

The Euler Deconvolution and analytical signal amplitude of magnetic anomalies over Ijero-Ekiti area have provided a rapid determination of the locations and depth estimates of the geologic structures (fault/fracture/ contacts and shear zones) that can be a host for rare earth minerals deposit in the investigated area. Analytic Signal Amplitude method has proven to be useful for locating the boundaries of geologic structures that is suspected to be mineralized in the investigated area. The Standard Euler Deconvolution method was very helpful not only in determination of the depths to the structural bodies, but also in delineating the boundaries/edges, extents and geometry of the geologic structures that can be targeted for rare earth mineralisation (lepidolite) within the investigated area.

The power spectral analysis of the aeromagnetic data revealed three depth source models. The shallow magnetic sources range in depth from about $< 10 - 50$ m. The depth to intermediate magnetic sources ranges from about 50–250 m while depth to the top of deepest magnetic source range from about 250–770 m in the study area. Therefore, it can be concluded in this study that interpretation of aeromagnetic data can rapidly yield geological structures that can be target for mineralization in the investigated area.

To enhance the imaging of deeper regional anomalies and facilitate residual separation, the data were first upward continued to a height of 12 km above mean sea level. The resulting regional field was then subtracted from the observed data to produce a residual aeromagnetic map emphasizing shallow magnetic sources and structures. For better visualization of intermediate-depth features, the residual aeromagnetic data were further upward continued to a height of 2000 meters. This workflow ensured consistent enhancement of both shallow and intermediate magnetic anomalies of interest across the study area. The 2-D geomagnetic sections imaged the subsurface and identified suspected fault/fracture (dykes and veins) that are indicative of mineralized pegmatite bodies along the profiles. The 2-D geomagnetic sections developed along the profiles delineated overburden thickness values which range from < 2.5–50 m and thickness values of geologic structures in the range of 375–1000 m across the investigated area.

The Euler Deconvolution and analytical signal amplitude of magnetic anomalies over lepidolite mineral deposits of Ijero-Ekiti area pegmatite field have provided information on the locations and depth estimates of the geologic structures (pegmatite dyke and veins) that can host rare earth minerals deposit in the investigated area without prior knowledge of the source geometry and magnetization direction. Analytic Signal Amplitude method has proven to be useful for locating the boundaries of geologic structures (lineaments) hosting the rare earth minerals (such as lepidolite) in the investigated area. The Standard Euler Deconvolution method was very helpful not only in determination of the depths to the lineaments hosting the mineralisation, but also in delineating the boundaries/edges, extents, internal geometry of the pegmatite bodies and the geologic structures controlling the rare earth mineralisation within the investigated area. The presence of existing mining sites along the lineaments further confirms the evidence of mineralisation of some of the geologic structures in the study area. This study concludes that the aeromagnetic survey data has been adequately utilized to develop the structural map of the investigated area.

Since the source parameters of the strong mine tremors were correlated and each correlation was similar to that of earthquakes, the stress drop, which can represent the environmental stress state of the source area of an event, was selected to compare the source parameter characteristics of earthquakes and mining tremors. The results show that the stress drops of the mining tremors were orders of magnitude lower than those of earthquakes, which reflects that a mining tremor generates a much lower background environmental stress than an earthquake. The mining tremors and earthquakes showed considerable differences in source parameter characteristics mainly due to their different specific physical mechanisms and the occurrence of mining tremors in the goafs.

In summary, the source parameters of strong mine tremors and earthquakes have both similarities and unique characteristics, which indicates that strong mine tremors and earthquakes have differences in their physical mechanisms.

In the future, we must monitor and evaluate mining tremors by learning from the theories and analysis methods of earthquakes while considering their differences from earthquakes.

Acknowledgement – The authors are grateful to Mr. A.A kinmola who assisted with the procurement of airborne magnetic dataset from Nigerian Geological Survey Agency (NGSA), Abuja, Nigeria.

Statements and declarations – The authors declare that there is no funding for this research. Additionally, there are no conflicts of interest.

References

Afolabi, D. O., Akinlalu, A. A. and Sanusi, S. O. (2024): Integrated geophysical and remote sensing investigations in hydrothermal mapping for orogenic gold mineralization in parts of Ife–Ilesa schist belt SW Nigeria – A case study, *Arab. J. Geosci.*, **17,** 244, https://doi.org/10.1007/s12517-024-12048-6.

Ajakaye,D. E., Halt, D. H., Millar, T. W., Verheljen, Award, M. B. and Ojo, S. B (1986): Aeromagnetic anomalies and tectonic trends in and around the Benue Trough, Nigeria, *Nature*, **319**(6054), 582–584, https://doi.org/10.1038/319582a0

Akande, S. O. and Fakorede, O. (1988): Gold mineralization in the Nigerian Schist Belts, **88**, Bicentennial Gold, Melbourne, 140–142.

Akinlalu, A. A., Olayanju, G. M., Adiat, K. A. N. and Omosuyi, G. O. (2021): Mineralization potential assessment using analytical hierarchy process (AHP) modeling technique: A case study of Ilesha schist belt, southwestern Nigeria, *Results Geophys. Sci.*, **7**, 100026, https://doi.org/10.1016/j.ringps.2021.100026.

Akinlalu, A. A. (2023): Radiometric mapping for the identification of hydrothermally altered zones related to Gold mineralization in Ife–Ilesa Schist belt, Southwestern Nigeria, *Indonesian J. Earth Sci.*, **3**(1), A519, https://doi.org/10.52562/injoes.2023.519.

Akinlalu, A. A., Afolabi, D. O. and Sanusi, S. O. (2024): Knowledge-driven fuzzy AHP model for orogenic gold prospecting in a typical schist belt environment: A mineral system approach, *Earth Syst. Environ.*, **8**, 221–263, https://doi.org/10.1007/s41748-024-00382-4.

Akinlalu, A. A. (2025). Exploration of iron ore deposits in parts of Kogi State, northcentral Nigeria: Analyses from airborne magnetic and ASTER datasets, *Geosystems and Geoenvironment*, **4**(2), 100359, https://doi.org/10.1016/j.geogeo.2025.100359.

Akinola, O. O, Okunlola, O. A. and Obasi, R. A. (2014): Physico-chemical characteristics and industrial potentials of lepidolite from Ijero-Aramoko pegmatite field, Southwestern Nigeria, *Int. J. Sci. Tech. Res.*, **3**(3), 278–284.

Alek, K. and Hamoudi, M. (2008): Regional-scale aeromagnetic survey of the south–west of Algeria: A tool for area selection for diamond exploration, *J. Afr. Earth Sci.*, **50**(2-4), 67–78, https://doi.org/10.1016/j.jafrearsci.2007.09.018.

Amigun, J. O., Afolabi, O. and Ako, B. D. (2012): Euler 3-D deconvolution of analytical signal of magnetic anomalies over iron deposit in Okene, Nigeria, *J. Eng. Trends Eng. Appl. Sci.* (*JETEAS*), **3**(4), 711–717, https://hdl.handle.net/10520/EJC126631.

Andongma, W. T., Gajere. J. N., Amuda. A. K., Edmond, R. R. D., Faisal, M. and Yusuf, Y. D. (2021): Mapping of hydrothermal alterations related to gold mineralization within parts of the Malumfashi Schist Belt, North-Western Nigeria, *Egypt. J. Rem. Sens. Space Sci.*, **24**(3/1), 401–417, https://doi.org/10.1016/j.ejrs.2020.11.001.

Bai, H., Cao, Y., Zhang, H., Zhang, C., Hou, S. and Wang, W. (2021): Combining fuzzy analytic hierarchy process with concentration–area fractal for mineral prospectivity mapping: A case study

involving Qinling orogenic belt in central China, *Appl. Geochem.*, **126**, 104894, 1–12, https://doi.org/10.1016/j.apgeochem.2021.104894.

Barbosa, V. C. F., Silva, J. B. C. and Medeiros, W. E (1999): Stability analysis and improvement of structural index estimation in Euler deconvolution, *Geophysics*, **64**(1), 48–60, https://doi.org/10.1190/1.1444529.

Bayode, S. and Akpoarebe, O. (2011): An integrated geophysical investigation of a spring in Ibuji, Igbara-Oke, Southwestern Nigeria, *Ife J. Sci.*, **13**(1), 63–74.

Bayode, S. (2013): Hydro-geophysical investigation of the federal housing estate Akure, Southwestern Nigeria, *J. Emerg Trends Eng. Appl. Sci.* (*JETEAS*), **4**(6), 793–799.

Bayode, S., Adeboye, J. O., Sanusi, S. O. and Akinlalu, A. A. (2023): Orogenic gold mineralization targeting of Alagbede Goldfield Southwestern Nigeria using an integrated geophysical approach, *Mining, Metallurgy & Exploration*, **40**, 955–983, https://doi.org/10.1007/s42461-023-00763-9.

Behera, S., Panigrahi, M. K. and Pradhan, A. (2019): Identifiation of geochemical anomaly and gold potential mapping in the Sonakhan Greenstone belt, Central India: An integrated concentration--area fractal and fuzzy-AHP approach, *Appl. Geochem.*, **107**, 45–57, https://doi.org/10.1016/j.apgeochem.2019.05.015.

Bhattacharya, B. K. (1966): Continuous spectrum of the total magnetic field anomaly due to a rectangular prismatic body, *Geophysics*, **31**(1), 97–121, https://doi.org/10.1190/1.1439767.

Blakely, R. J. (1996): *Potential theory in gravity and magnetic applications*. Cambridge University Press, Cambridge, England, 441 pp, https://doi.org/10.1017/CBO9780511549816.

Briggs, I. (1974): Machine contouring using minimum curvature, *Geophysics,* **39**(1), 39–48, https://doi.org/10.1190/1.1440410.

Cheyney, S., Hill, I. A. and Linford, N. (2011): Advantages to using the pseudo-gravity transformation to aid edge detection of total field archaeo-magnetic datasets, *Archaeol. Prospect.*, **18**(2), 81–93, https://doi.org/10.1002/arp.408.

Cooper, G. R. J. (2004): Euler deconvolution applied to potential field gradients, *Explor. Geophys.*, **35**(3), 165–170, https://doi.org/10.1071/EG04165.

Cooper, G. R. J. and Cowan, D. R. (2008): Edge enhancement of potential field data using normalised statistics, *Geophysics*, **73**(3), H1–H4, https://doi.org/10.1190/1.2837309.

Durrheim, R. J and Cooper, G. R. J. (1998): Euldep, a program for the Euler deconvolution of magnetic and gravity data, *Comput. Geosci.*, **24**(6), 545–550, https://doi.org/10.1016/S0098-3004(98)00022-3.

Eberle, D. G., Daudi, E. X. F, Muiuane, E. A., Nyabeze, P. and Pontavida, A. M. (2012): Crisp clustering of airborne geophysical data from the Alto lingonha pegmatite field, northestern Mozambique, to predict zones of increased rare earth element potential, *J. Afr. Earth Sci.*, **62**, 26–34, https://doi.org/10.1016/j.jafrearsci.2011.08.003.

Ekwok, S. E., Achadu, O. I. M., Akpan, A. E., Eldosouky, A. M., Ufuafuonye, C. H., Abdelrahman, K. and Gómez-Ortiz, D. (2022a): Depth estimation of sedimentary sections and basement rocks in the Bornu Basin, Northeast Nigeria using high-resolution airborne magnetic data, *Minerals*, **12**(3), 285, https://doi.org/10.3390/min12030285.

Eldosouky, A. M., Abd El Wahed, M. A. and Saada, S. A. (2025): New insights into structural and tectonic evolution of Safaga-Semna shear belt, Eastern Desert, Egypt: Advanced integration of aeromagnetic, remote sensing and field studies, *Geomech. Geophys. Geo-energ. Geo-resour.*, **11**, 31, https://doi.org/10.1007/s40948-025-00946-2.

Eldosouky, A. M., Eleraki, M., Mansour, A., Saada, S. A. and Zamzam, S. (2024): Geological controls of mineralization occurrences in the Egyptian Eastern Desert using advanced integration of remote sensing and magnetic data, *Sci. Rep.-UK,* **14**, 16700, https://doi.org/10.1038/s41598-024-66924-y.

Eldosouky, A. M., Othman, A., Saada, S. A. and Zamzam, S. (2024a): A new vector for mapping gold mineralization potential and proposed pathways in highly weathered basement rocks using multispectral, radar, and magnetic data in random forest algorithm, *Nat. Resour. Res.*, **33**, 23–50, https://doi.org/10.1007/s11053-023-10292-3.

El-Dawi, M. G, Tianyou, L., Hui, S. and Dapeng, L. (2004): Depth estimation of 2-D magnetic anomalous sources by using Euler deconvolution method, *Am. J. Appl. Sci.*, **1**(3), 209–214.

Fieberg, F. C. (2002): Ground magnetic investigations for gold prospecting in south-western Nigeria, *Presentation given at the 62nd Meeting of the German Geophysical Socieity*, Hannover, Germany, 4 February 2002, 20.

Forson, E. D., Menyeh, A., Wemegah, D. D., Danuor, S. K., Adjovu, I. and Appiah, I. (2020): Mesothermal gold prospectivity mapping of the southern Kibi-Winneba belt of Ghana based on fuzzy analytical hierarchy process, concentration area (C-A) fractal model and prediction-area (P-A) plot, *J. Appl. Geophys.*, **174**, 103971, https://doi.org/10.1016/j.jappgeo.2020.103971.

Geosoft (2007): *Geosoft Oasis Montaj – Mapping and Application System Inc.*, Suit 500, Richmond St. West Toronto, ON, Canada, N5SIV6.

Gunn, A, G., Dorbor, J. K., Mankelow, J. M., Lusty, P. A. J., Deady, E. A., Shaw, R. A. and Goodenough, K. M. (2018): A review of mineral potential of Liberia, *Ore Geol. Rev.*, **101**, 413–431, https://doi.org/10.1016/j.oregeorev.2018.07.021.

Keating, P. and Zerbo, L. (1996): An improved technique for reduction to the pole at low latitudes, *Geophysics*, **61**(1), 131–137, https://doi.org/10.1190/1.1443933.

KPMG - Klynveld Peat Marwick Goerdeler (2017): *Nigeria Mining Sector Brief*. Third Edition, 32 pp.

Langenheim, V. E., and Jachens, R. C. (2014): Aeromagnetic data, processing, and maps of Fort Irwin and vicinity, California, in: *Geology and geophysics applied to groundwater hydrology at Fort Irwin, California – Chapter I*, edited by Buesch, D. C. U.S. Geological Survey Open-File Report 2013–1024, 18 p, https://dx.doi.org/10.3133/ofr20131024i.

Li, X. (2006): Understanding 3-D analytic signal amplitude, *Geophysics*, **71**(2), L13–L16, https://doi.org/10.1190/1.2184367.

Lowrie, W. (2007): *Fundamentals of geophysics*. Cambridge University Press, Cambridge, UK, X+381 pp, https://doi.org/10.1017/CBO9780511807107.

Li, Z., He, M. Y., Li, B., Wen, X., Zhou, J., Cheng, Y., Zhang, N. and Deng, L. (2024a): Multi-isotopic composition (Li and B isotopes) and hydrochemistry characterization of the Lakko Co Li-rich salt lake in Tibet, China: Origin and hydrological processes, *J. Hydrol.*, **630**, 130714, https://doi.org/10.1016/j.jhydrol.2024.130714.

Liu, G., Meng, H., Song, G., Bo, W., Zhao, P., Ning, B. and Xu, X. (2024a): Numerical simulation of wedge failure of rock slopes using three-dimensional discontinuous deformation analysis, *Environ. Earth Sci.*, **83**(10), 310, https://doi.org/10.1007/s12665-024-11619-w.

Liu, Y., Yang, D., Li, Y., Cai, J. and Jiang, X. (2024b): Nanoindentation study on microscopic mineral mechanics and bedding characteristics of continental shales, *Energy*, 27 pp, https://doi.org/10.2139/ssrn.4712842.

Liu, Y.-X., Li, W.-Y., Liu, Z.-Y., Zhao, J.-W., Cao, A.-Q., Gao, S., Wang, L.-J. and Yang, C. (2022): Occurrence characteristics of magnetite and aeromagnetic prospecting northeast of Hebei Province, *Minerals*, **12**, 1158, https://doi.org/10.3390/min12091158.

MacLeod, I. N., Jones, K. and Dai, T. F. (1993a): 3-D analytic signal in the interpretation of total magnetic field data at low magnetic latitudes, *Explor. Geophys.*, **24**, 679–688, https://doi.org/10.1071/EG993679.

MacLeod, I. N., Vierra, S. and Chaves, A. C. (1993): Analytic signal and Reduction-to-the-Pole in the interpretation of the total magnetic field data at low magnetic latitudes, in: *Proceedings of the third international congress of the Brazilian Society of Geophysicists*, Rio de Janeiro, Brazil, 7–11 November 1993, cp-324-0158, https://doi.org/10.3997/2214-4609-pdb.324.830.

Mahdi, A. M., Youssef, A. M., Gabr, S. S., Diab, H. I., Alarifi, S. S., Andráš, P. and Eldosouky, A. M. (2025): Exploring potential mineral deposits: Integrating airborne magnetic and remote sensing data in North-eastern Desert, Egypt, *Adv. Space Res.*, **75**(6), 4472–4489, https://doi.org/10.1016/j.asr.2024.12.043.

Matende, K. N., Ranganai, R. T., Mickus, K. L., Lelievre, P. G., Mapeo, R. B. M. and Ramotoroko, C. D. (2023): Geophysical and geological investigations of the spatial and subsurface extent of the

Segwagwa and Masoke igneous ring complexes in southeast Botswana: Geotectonic implications. *J. Afr. Earth Sci.*, **197**, 104766, https://doi.org/10.1016/j.jafrearsci.2022.104766.

Mushayandebvu, M. F., van Driel, P., Reid, A. B. and Fairhead, J. D. (1999): Magnetic imaging using extended Euler deconvolution, *Presented at the 69th Ann. Internat. Mtg., Soc. Expl. Geophys.*, https://doi.org/10.1190/1.1821035.

Miller, H. and Singh, V. (1994): Potential field tilt—A new concept for location of potential field sources, *J. Appl. Geophys.*, **32**(1), 213–217, https://doi.org/10.1016/0926-9851(94)90022-1.

Nabighian, M. N. (1972): The analytic signal of two-dimensional magnetic bodies with polygonal cross-section: Its properties and use for automated anomaly interpretation, *Geophysics*, **37**, 507–517, https://dx.doi.org/10.1190/1.1440276.

Obaje, N. G. (2009): *Geology and mineral resources of Nigeria*. Springer, London, Dordrecht, Berlin, 221 pp, https://doi.org/10.1007/978-3-540-92685-6.

Odeyemi, I. B. (1976): Preliminary report on the field relationships of the basement complex rocks around Igarra, Midwest Nigeria, in: *Geology of Nigeria*, edited by: Kogbe, C. A. Elizabethan Publishing Co., Lagos, 59–63 pp.

Okunlola, O. A. and Akinola, O. O. (2010): Petrochemical characteristics of the Precambrian rare metal pegmatite of Oke-Asa area, Southwestern Nigeria: Implication for Ta-Nb mineralization, *RMZ – Materials and Geoenvironment*, **57**(4), 525–538.

Oladunjoye, M. A., Olayinka, A. I., Alaba, M. and Adabanija, M. A. (2016): Interpretation of high resolution aeromagnetic data for lineaments study and occurrence of Banded Iron Formation in Ogbomoso area, Southwestern Nigeria, *J. Afr. Earth Sci.*, **114**, 43–53, https://doi.org/10.1016/j.jafrearsci.2015.10.015.

Olade, M. A. (2019): Geological re-evaluation of Nigeria's iron ore deposits as raw materialsfor a viable iron and steel industry, *Achievers J. Scient. Res.*, **2**(1), 1–22.

Olayanju, G. M. (2015): Geophysical mapping of the inland extension of deep ocean fault zones, Southwestern Nigeria, *J. Earth Sci. Res.*, **4**(2), 45–62, https://doi.org/10.5539/esr.v4n2p45.

Olayanju, G. M., Akinlalu, A. A., Adiat, A. A., Asowata, I. T., Akinwunmiju, A. S., Afolabi, D. O. and Olomo, K. O. (2024): Delineating hydrothermal alterations relating to primary gold mineralization using airborne radiometric and remote sensing datasets in Ilesha Schist Belt, Southwestern Nigeria, *J. Earth Sci. Res.*, **7**(1), 14–38.

Olomo, K. O., Olayanju, M. O., Bayode, S., Alagbe, O. A. and Olaleye, O. K. (2024): Electrical and electromagnetic geophysical signature associated with geological frame of polymineralic deposit within hydrothermal alteration zones, *J. Appl. Geophys.*, **222**, 105315, https://doi.org/10.1016/j.jappgeo.2024.105315.

Ordóñez, C., Ekwok, S. E., Alkhayaat, A., Bains,P. S., Sharma, R., Kumar, R., Kulshreshta, A., Mann, V. S. and Elmasry, Y. (2024): Delineation of mineralization-related geologic structures and lithological units using airborne magnetic and radiometric data, *Geomech. Geophys. Geo-energ. Geo-resour.*, **10**, 184, https://doi.org/10.1007/s40948-024-00902-6.

Piro, S., Sambuelli, L., Godio, A. and Taormina, R. (2007): Beyond image analysis in processing archaeomagnetic geophysical data: Case studies of chamber tombs with dromos, *Near Surf. Geophys.*, **5**, 405–414, https://doi.org/10.3997/1873-0604.2007023.

Panisova, J. and Pasteka, R. (2009): The use of microgravity technique in archaeology: A case study from the St. Nicolas Church in Pukanec, Slovakia, *Contrib. Geophys. Geodesy*, **39**(3), 237–254, https://doi.org/10.2478/v10126-009-0009-1.

Patra, A. K, Chaturvedi, P. K. and Ramyya, M. S. (2013): Integrated interpretation of satelite imagery, aeromagnetic, aeroradiometric and ground exploration data-sets to delineate favourable target zones for unconformity related uranium mineralization, Khariar Basin, central India, *J. Geol. Soc. India*, **81**, 299–308, https://doi.org/10.1007/s12594-013-0041-7.

Parlowski, J., Lewis, R., Dobush, T. D. and Valleau, N. (1995): An integrated approach for measuring and processing geophysical data for the detection of unexploded ordnance, in: *Proceedings of Symposium on the Application of Geophysics to Engineering and Environmental Problems* (*SAGEEP1995*), 965–974.

Reid, A. B., Allsop, J. M., Granser, H., Millett, A. J. and Somerton, I. W. (1990): Magnetic interpretation in three dimensions using Euler deconvolution, *Geophysics*, **55**, 80–91, https://doi.org/10.1190/1.1442774.

Reid, A. B. (1995): Euler deconvolution: Past, present and future – A review, *65th SEG Meeting*, Houston, USA, Expanded Abstract, 272–273.

Reynolds, J. M. (1997): *Introduction to applied and environmental geophysics*. First Edition, Pbl., Wiley, London, pp. 187.

Reeves, C. V. (2005): *Aeromagnetic surveys: Principles, practice and interpretation*. Earth-works, Washington DC, 155 p.

Riahi, S., Bahroudi, A., Abedi, M., Aslani, S. and Lentz, D. R. (2022): Evidential data integration to produce porphyry Cu prospectivity map, using a combination of knowledge and data–driven methods, *Geophys. Prospect.*, **70**(2), 421–437, https://doi.org/10.1111/1365-2478.13169.

Roest, W. R., Verhoef, J. and Pilkington, M. (1992): Magnetic interpretation using the 3D analytic signal, *Geophysics*, **57**(1), 116–125, https://doi.org/10.1190/1.1443174.

Saad, S., Alarifi, S. S., El-Qassas, R. A. Y., Omar, A. E. A., Ahmad, M., Al-Saleh, A. M., Andráš, P. and · Eldosouky, A. M (2024): Remote sensing and aeromagnetic mapping for unveiling mineralization potential: Nuqrah Area, Saudi Arabia, *Geomech. Geophys. Geo-energ. Geo-resour.*, **10**, 149, https://doi.org/10.1007/s40948-024-00844-z.

Sanusi, S. O. and Amigun, J. O. (2020): Structural and hydrothermal alteration mapping related to orogenic gold mineralization in part of Kushaka schist belt, North-central Nigeria, using airborne magnetic and gamma-ray spectrometry data, *SN Appl. Sci.*, **2**(9), 1591, https://doi.org/10.1007/s42452-020-03435-1.

Sanusi, S. O., Olaniyan, O., Afolabi, D. O. and Olayanju, G. M. (2024): Mapping orogenic gold mineralization potential in the Kushaka Schist belt, Northcentral Nigeria: Insights from point pattern, kernel density, Staged – Factor, and fuzzy AHP modeling techniques, *Earth Syst. Environ.*, **9**, 135–184, https://doi.org/10.1007/s41748-024-00427-8.

Spector, A. and Grant, F. S. (1970): Statistical models for interpreting aeromagnetic data, *Geophysics*, **35**(2), 293–302, https://doi.org/10.1190/1.1440092.

Telford, W. M., Geldart, L. P. and Sheriff, R. E. (1990): *Applied geophysics*. 2nd Edition, Cambridge University Press, Cambridge, UK, 770 pp, https://doi.org/10.1017/CBO9781139167932.

Thompson, D. T. (1982): EULDPH – A new technique for making computer-assisted depth estimates from magnetic data, *Geophysics*, **47**, 31–37, https://doi.org/10.1190/1.1441278.

Uruc, B. and Selim, H. H. (2011): Interpretation of magnetic data in the Sinop area of Mid Black Sea, Turkey, using tilt derivative, Euler deconvolution, and discrete wavelet transform, *J. Appl. Geophys.*, **74**, 194–204, https://doi.org/10.1016/j.jappgeo.2011.05.007.

Wemegah, D. D., Preko, K., Noye, R. M., Boadi, B., Menyeh, A. Danuor, S. K. and Amenyoh, T. (2015): Geophysical interpretation of possible gold mineralization zones in Kyerano, South-Western Ghana using aeromagnetic and radiometric datasets, *J. Geosci. Environ. Protect.*, in: *Sci. Res.*, **3**, 67–82, https://doi.org/10.4236/gep.2015.34008.

Wijns, C., Perez, C. and Kowalczyk, P. (2005): Theta map: Edge detection in magnetic data, short note, *Geophysics*, **70**(4), 39–43, https://doi.org/10.1190/1.1988184.

Yousefi, M. and Carranza, E. J. M. (2016): Data–driven index overlay and Boolean logic mineral prospectivity modeling in green fields exploration, *Nat. Res.*, **25**, 3–18, https://doi.org/10.1007/s11053-014-9261-9.

Zouaghi, T. and Harbi, H. (2022): Airborne geophysics and remote sensing of an Nimas – Khadra area, Southern Arabian shield: New insights ito structural framework and mineral resources, *Adv. Space Res.*, **70**, 3649–3673, https://doi.org/10.1016/j.asr.2022.08.046.

SAŽETAK

Strukturno-geološko kartiranje potencijalne prisutnosti rijetkih zemnih minerala pomoću aeromagnetskih podataka

Sunday Bayode, Folahan Peter Ibitoye i Ayokunle Adewale Akinlalu

Primjena aeromagnetskih anomalija u istraživanju rijetkih zemnih minerala (lepidolit) u pegmatitnom polju Ijero-Aramoko, jugozapadna Nigerija, provedena je s ciljem određivanja lokacija i dubina lineamenata koji sadrže pegmatitna tijela. Korištena metodologija uključivala je tehniku Eulerove dekonvolucije primijenjenu na 2D profile i interpolirane podatke o potencijalnom polju kako bi se dobile procjene lokacija i dubina minerala. U ovom istraživanju primijenjeno je vertikalno prosljeđivanje (upward continuation) kako bi se aeromagnetski podaci, izvorno izmjereni na visini leta od približno 100 metara iznad razine tla, transformirali na visinu od 400 metara iznad razine mora. Ovaj postupak omogućio je zanemarivanje vrlo plitkih izvora i pozadinske buke, čime je poboljšano prikazivanje relevantnih plitkih magnetskih izvora (struktura) i anomalija od interesa na rezidualnoj aeromagnetskoj karti. 2D geomagnetski presjeci izrađeni duž dviju presječnih linija preko istraživanog područja razgraničili su sumnjive zone rasjeda/pukotina koje se odlikuju niskom magnetskom susceptibilnosti. Eulerova dekonvolucija primijenjena je na podatke s vrijednostima strukturnih indeksa (SI) 0,5, 1 i 2. Eulerova rješenja za strukturne indekse i analiza spektra snage dale su dubine koje se kreću od manje od 10 do 50 m za plitke izvore, 50–250 m za srednje duboke magnetske izvore te 250–770 m za dublje izvore. Najbolja rješenja dala su Eulerova rješenja za strukturne indekse 0,5 i 1,0. Rezultati ovog istraživanja pokazali su da mineralizacija rijetkih zemnih elemenata bogata pegmatitom postoji kao magnetski izvor s niskim magnetskim intenzitetom na relativno plitkoj dubini. Postojanje rudarskih lokacija u blizini lineamenata dodatno potvrđuje dokaze o mineralizaciji nekih od geoloških struktura razgraničenih u istraživanom području.

Ključne riječi: lepidolit, Eulerova dekonvolucija, aeromagnetično, minerali rijetkih zemalja

Corresponding author's address: Ayokunle Adewale Akinlalu, Department of Applied Geophysics, Federal University of Technology, Akure, Ondo State, Nigeria; e-mail: aaakinlalu@futa.edu.ng